Supporting Information

Trapping of protein cargo molecules inside DNA origami nanocages

Merle Scherf [a,b], Florian Scheffler [a,b], Christopher Maffeo [c], Ulrich Kemper [b], Jingjing Ye [b,d], Aleksei Aksimentiev [c,e], Ralf Seidel [b,d] and Uta Reibetanz *[a]

a Institute for Medical Physics and Biophysics, Medical Faculty, University of Leipzig, Härtelstraße 16-18, 04107 Leipzig, Germany

b Peter Debye Institute for Soft Matter Physics, Faculty of Physics and Earth Science, University of Leipzig, Linnéstraße 5, 04103 Leipzig, Germany

c Department of Physics, University of Illinois at Urbana–Champaign, 1110 W Green St, Urbana, IL 61801, USA

d Cluster for Advancing Electronic Devices Dresden, University of Dresden, Helmholtzstraße 18, 01069 Dresden, Germany

e Beckman Institute for Advanced Science and Technology, University of Illinois at Urbana–Champaign, 405 N Mathews Ave, Urbana, IL 61801, USA

KEYWORDS DNA origami nanocages, freely diffusing molecules, drug delivery, coarse-grained simulations

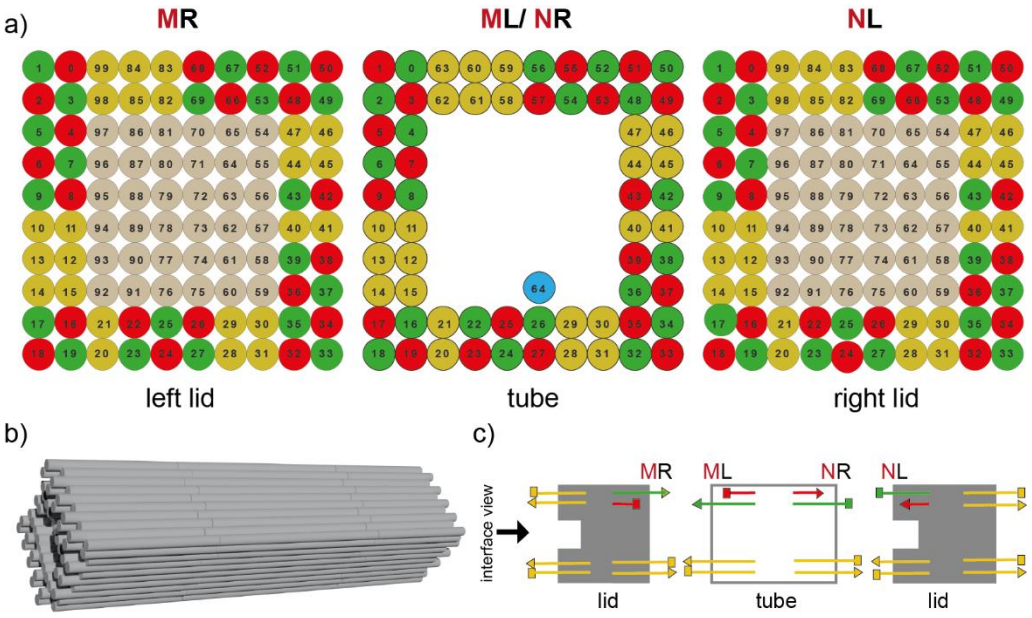

Figure S1 - Interface design for DNA origami cages.

a) Distribution of the attractive (red and green circles) and repulsive DNA ends (yellow circles) of the lid-tube interfaces for the left lid (interface MR), the tube (interfaces ML/NR) and the right lid (interface NL). The views on the interfaces are done from the left to right side of the final nanocage, as visualized in c). Beige circles inside the lids mark repulsive DNA ends that do not interact with the tube. The blue circle inside the tube marks the target strand inside the tube cavity. **b)** Three-dimensional scheme of the nanocage structure with tight connections between the tube and the lids, where each gray cylinder represents a DNA helix. The protrusion of the DNA ends of the lids matches the recession of the DNA ends of the tubes and vice versa, to support a tight docking of the lids onto the tube. **c)** Two-dimensional scheme of the DNA origami cage to illustrate the three different types of DNA ends for allowing specific binding and stable cage formation. Attractive DNA ends at the MR/ML interface are formed by 2 nt 3' staple extension and 5' staple recessions, while attractive DNA ends at the NL/NR are formed by 2 nt 5' staple extensions and 3' staple recessions (see red and green staples in the scheme, 5' ends and 3' ends are shown as squares and triangles, respectively). Repulsive DNA ends are obtained by -TACACT overhangs at 3' and 5' staple ends (see yellow staples). At the non-interacting sides of the lids only repulsive overhangs are present. The black arrow marks the viewing direction onto the interfaces in a).

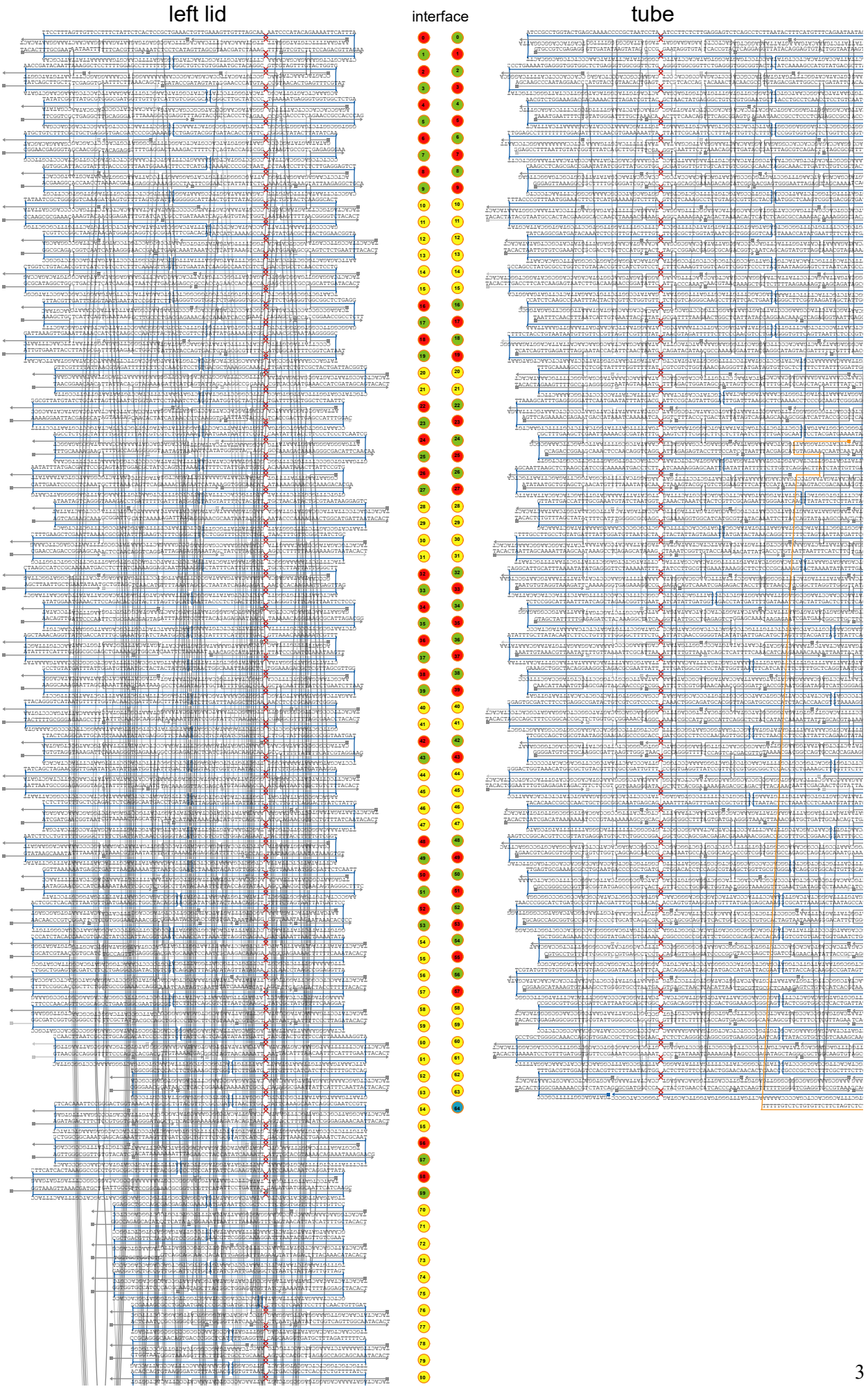
left lid
interface
tube

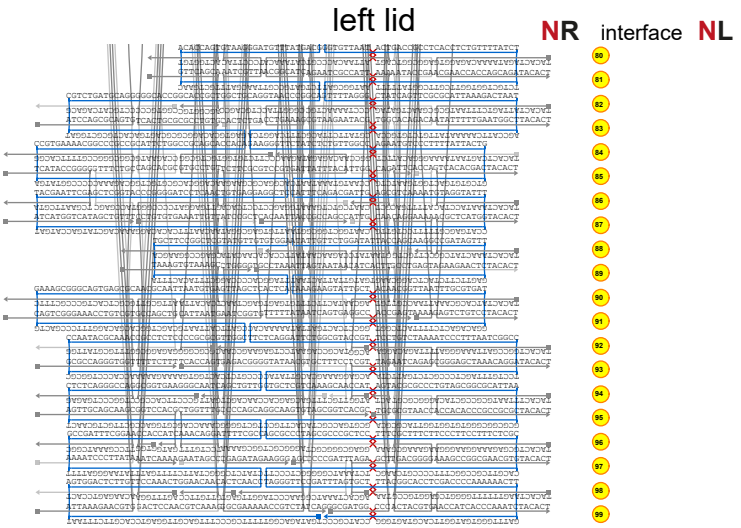

Figure S2 – Design templates of the left side of the origami nanotube and of the left lid in its original version.

The blue lines show the routing of the scaffolds p8064 with complementary staples in grey. The orange line (starting at helix 24) represents the staple that carries the target strand sequence as a 3'-overhang. Attractive helices ends with 2 nt recessions or extensions are marked with red or green circles, respectively. Yellow circles mark the repulsive helix ends with TACACT overhang. The blue circle in helix 64 marks the 3' overhang of the target strand that protrudes inside the cavitiy of the tube. Red crosses are introduced as imaginary gaps for the graphical illustration. The design is based on a square lattice of DNA helices.

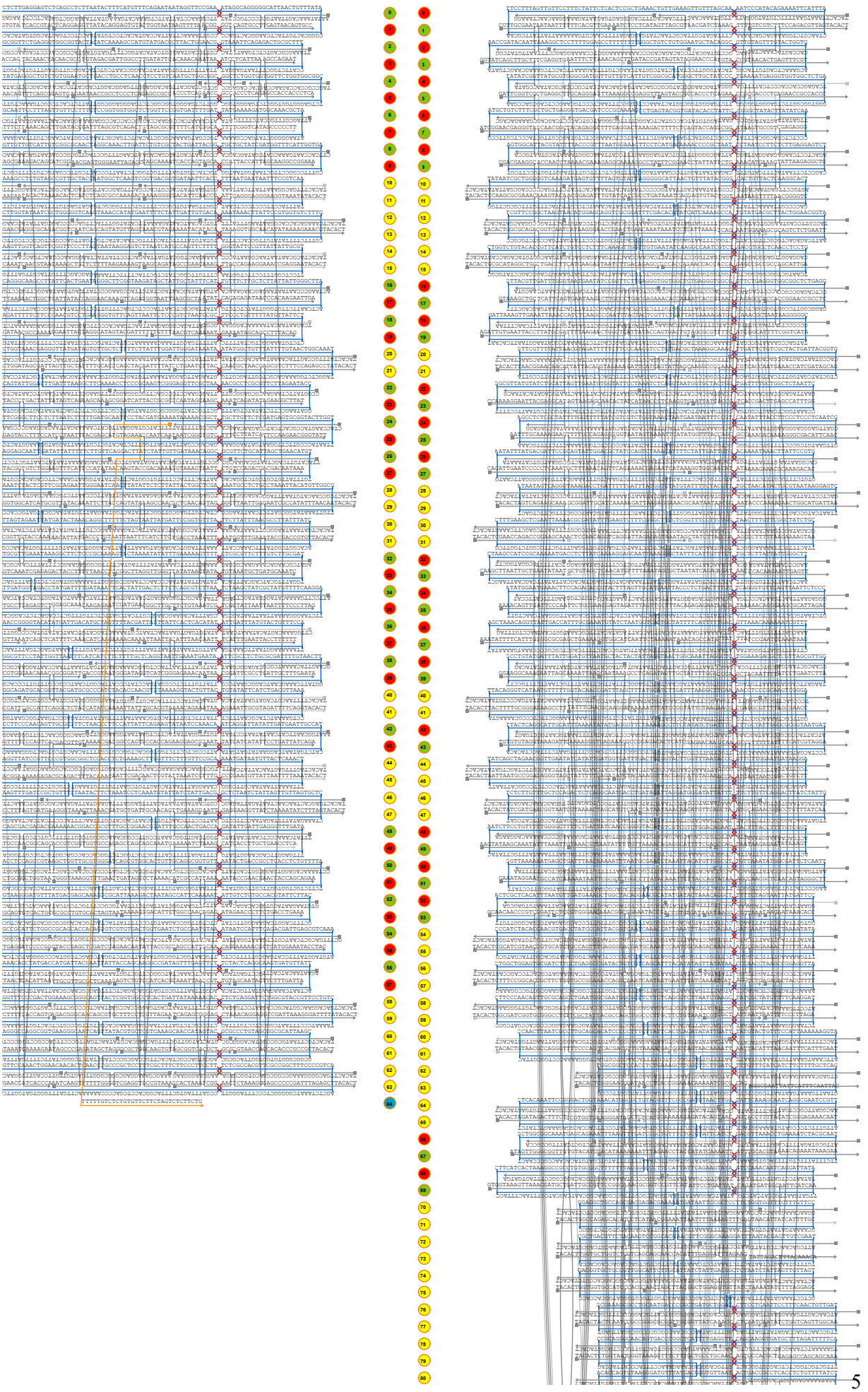
tube
NR interface NL
right lid

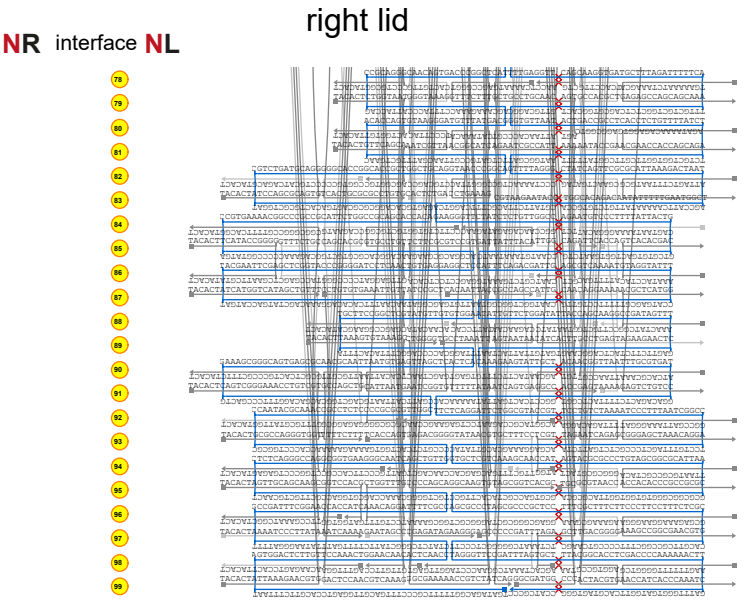

Figure S3 – Design templates of the right side of the origami nanotube and of the right lid in its original version.

The blue lines show the routing of the scaffolds p8064 with complementary staples in grey. The orange line (starting at helix 24) represents the staple that carries the target strand sequence as a 3'-overhang. Attractive helices ends with 2 nt recessions or extensions are marked with red or green circles, respectively. Yellow circles mark the repulsive helix ends with TACACT overhang. The blue circle in helix 64 marks the 3' overhang of the target strand that protrudes inside the cavitiy of the tube. Red crosses are introduced as imaginary gaps for the graphical illustration. At the right side of the lid only repulive ends are present as shown in the first two lines. The design is based on a square lattice of DNA helices.

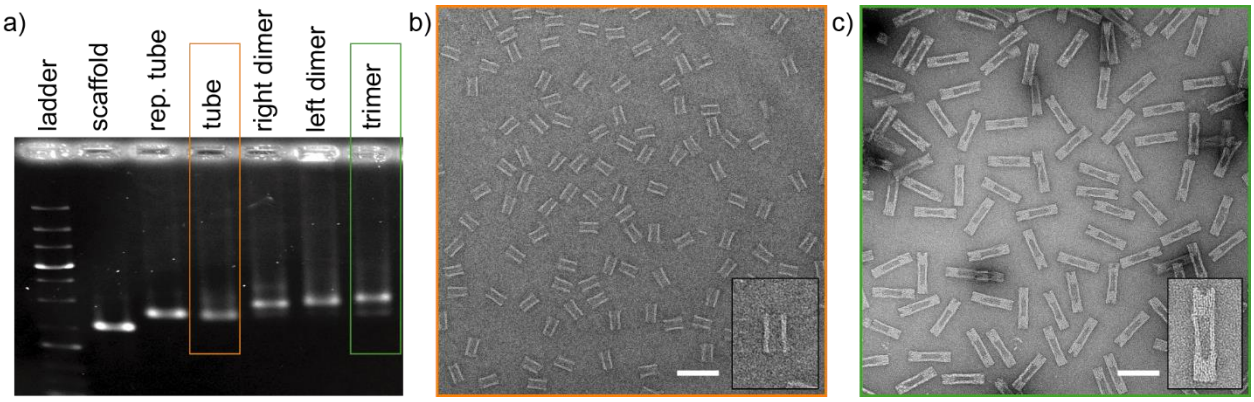

Figure S4 - Analysis of the nanocage assembly.

a) Analysis of nanocage assembly by agarose gel electrophoresis and subsequent ethidium bromid staining. Individual lanes contain (from left to right): a DNA size marker, the p8064 scaffold DNA, a tube monomer that contains only repulsive DNA ends at both sides, the tube monomer with interfaces for lid binding at either side (see Figure S1), dimers of the tube with either the left or the right lid and the full trimeric nanocage assembly (see legend). From the samples marked with a orange and a green box, TEM images are shown on the left. **b)** TEM overview image of the tube sample with interfaces for lid binding reveals only individual monomers but no oligomers. **c)** TEM overview image of the nanocage assembly sample revealing a highly efficient cage formation. Scales bars correspond to 100 nm.

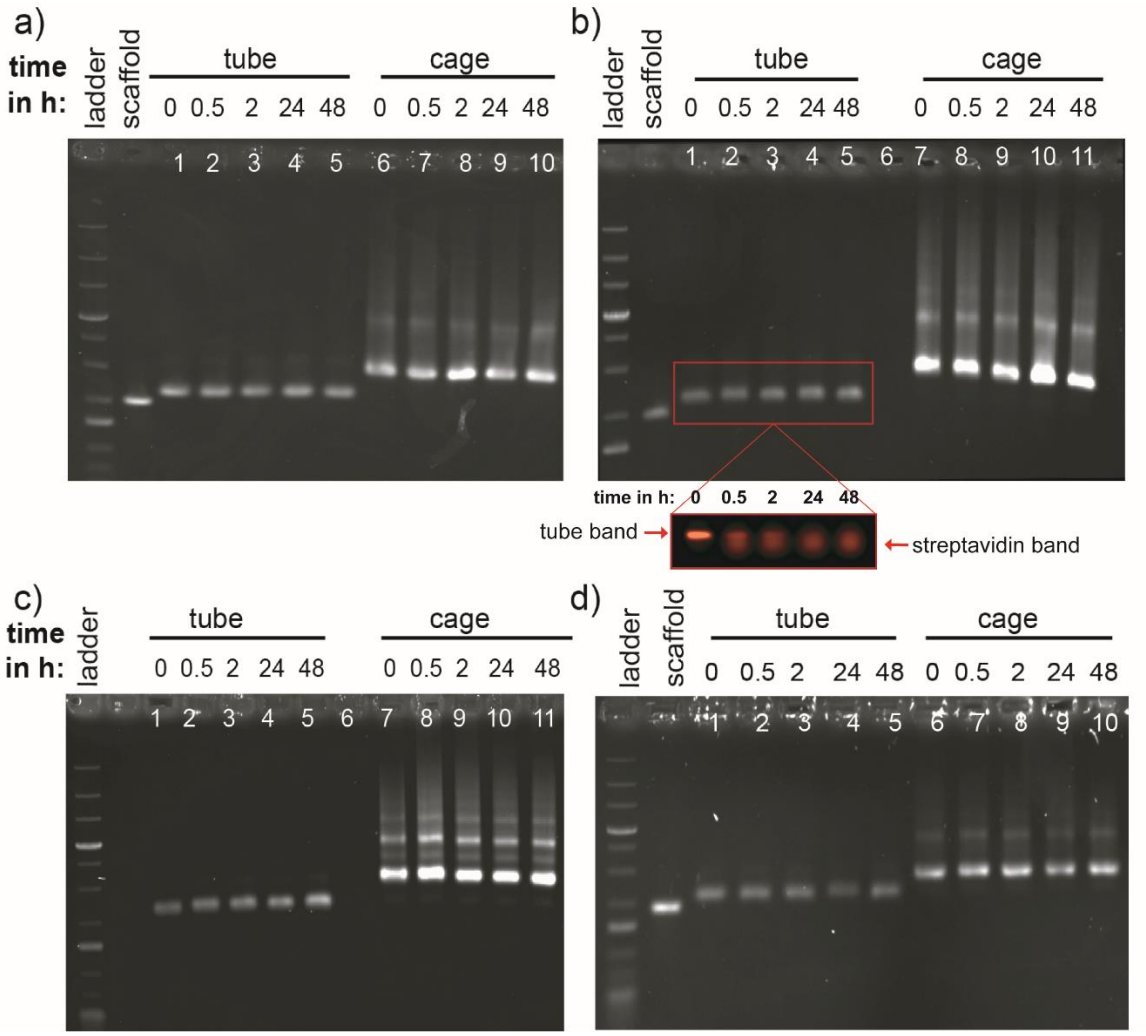

Figure S5 – Visualizing the total DNA amount and stability of DNA tubes and cages in agarose gels of strand displacement experiments using ethidium bromide staining.

After imaging the Cy3 or Cy5 fluorescence, the total DNA amount in the gels was visualized using ethidium bromide staining to verify an equal loading of tube and cage structures in all comparable lanes. Shown are the agarose gels for the displacement reactions between **a)** ssDNA invader and incumbent strands (see Figure 2), **b)** ssDNA invaders and streptavidin-conjugated incumbent strand (see Figure 3), **c)** streptavidin-conjugated invaders and ssDNA incumbents (see Figure 4) and **d)** ssDNA invaders and BSA conjugated incumbent strands (see Figure 5). Note that the DNA content per lane is three times higher for the cages than for the tubes due to the addition of the lids. Additional, in b) a cut-off of an unpurified gel image detecting Cy5 fluorescence, to visualize the overlapping tube and streptavidin band is shown.

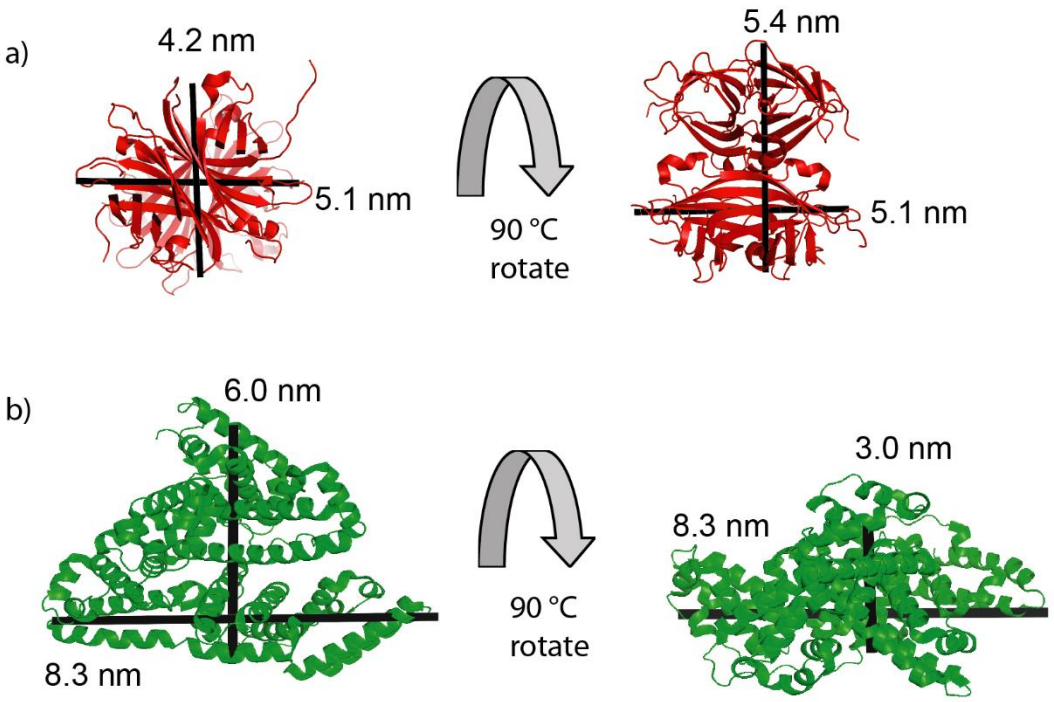

Figure S6 – Dimensions of streptavidin and BSA.

a) Crystal structure of streptavidin (PDB: 3ry1) shown for two orthogonal directions with indicated dimensions of about 4.2 × 5.1 × 5.4 nm **b)** Crystal structures of bovine serum albumin (BSA, PDB: 4f5s) shown for two orthogonal directions with indicated dimensions of approximately 8.3 × 6.0 × 3.0 nm. Both structures were visualized using Pymol (The pymol molecular graphics system, version 2.0, Schrödinger, LLC: New York, 2020. http://www.pymol.org (accessed 2022-05-15)).

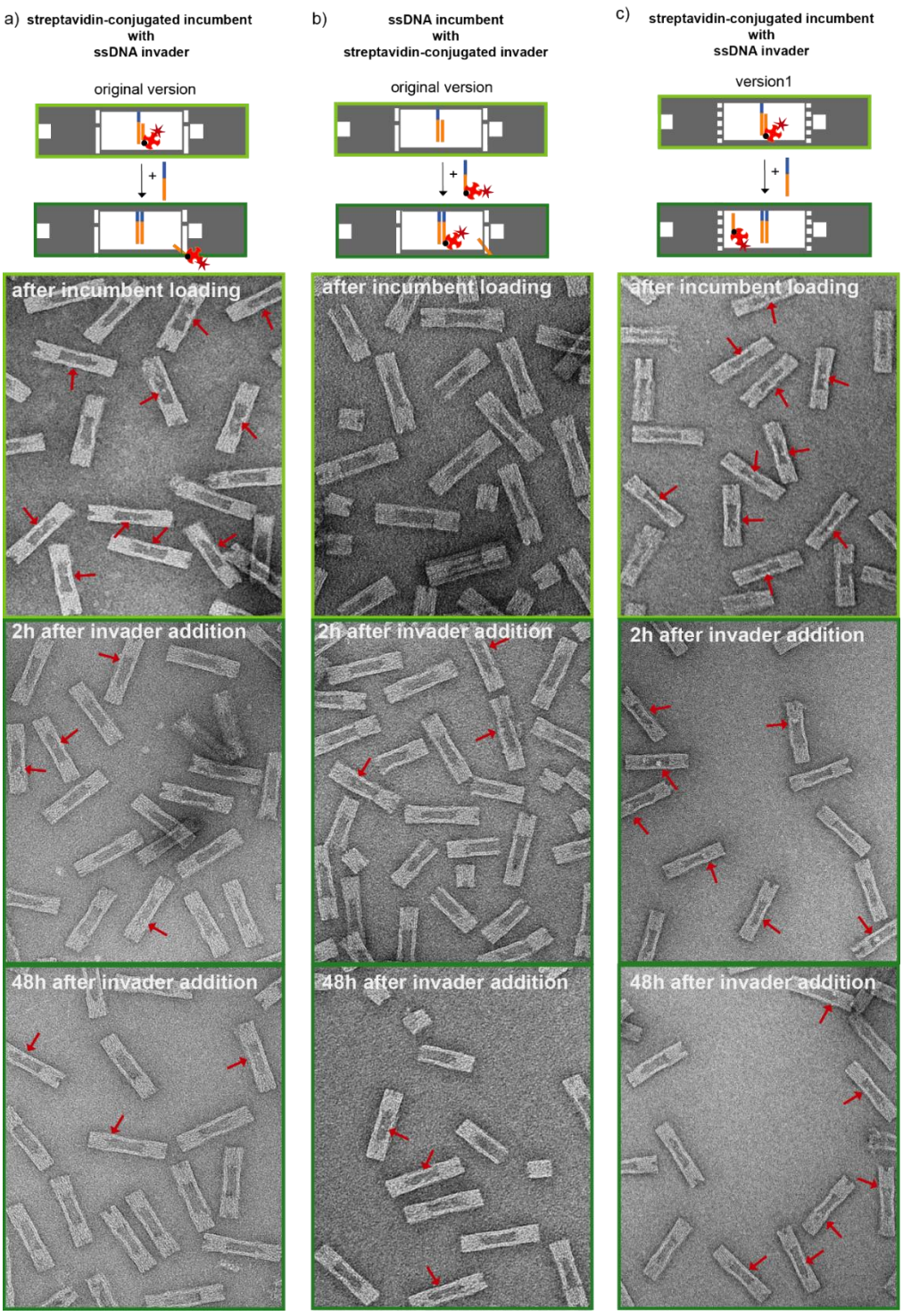

Figure S7 – TEM overview images of the DNA origami nanocages after incumbent loading and 2 h and 48 h after external addition of the invader.

Each column shows a scheme of the reaction with the incumbent and invader strands used in this particular reaction. The TEM images show the nanocages after incumbent loading (top) as well as 2 h (middle) and

48 h (bottom) after external addition of the invader. Red arrows mark streptavidin-cargo molecules inside the origami nanocages. **a)** Displacement of streptavidin-conjugated incumbents inside the original cage version by ssDNA invaders (see Figure 3). The initially bound streptavidin-incumbents disappear upon strand displacement by the DNA invader addition due to their escape through the cage walls. **b)** Displacement of ssDNA-incumbents bound inside the original cage version by streptavidin-conjugated invaders (see Figure 4). Streptavidin molecules appear only slowly with time inside the nanocages. **c)** Displacement of streptavidin-conjugated incumbent inside nanocage version 1 with tighter tube-lid connections by ssDNA invaders (see Figure 7). Some of the initially bound streptavidin-incumbents disappear upon DNA invader addition due to their escape through the cage walls. Compared to a), significantly more streptavidin molecules are retained inside the cages.

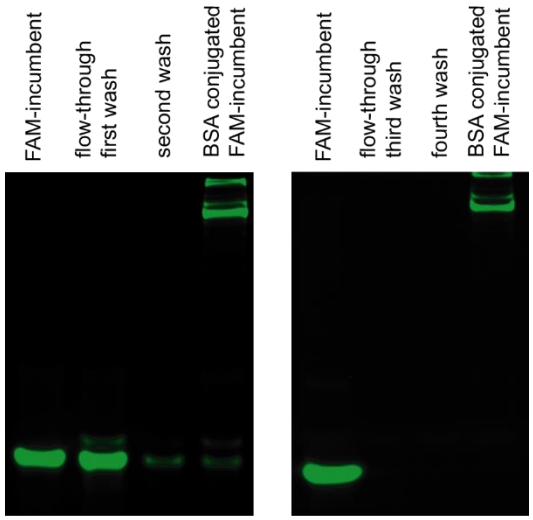

Figure S8 – Analysis of the conjugation of BSA with ssDNA incumbents.

Native polyacrylamide gel electrophoresis of the conjugation of BSA with the FAM-incumbent to visualize the complete removal of unbound incumbent by a 30 kDa Cut-Off filter (see Experimental). The lanes contain the FAM-labeled incumbent, the flow-through after the four different purification steps and the finally purified conjugated BSA sample. After the first two washing steps unbound FAM-incumbents are still visible (left gel which are not detected anymore after the third and fourth washing steps (right gel).

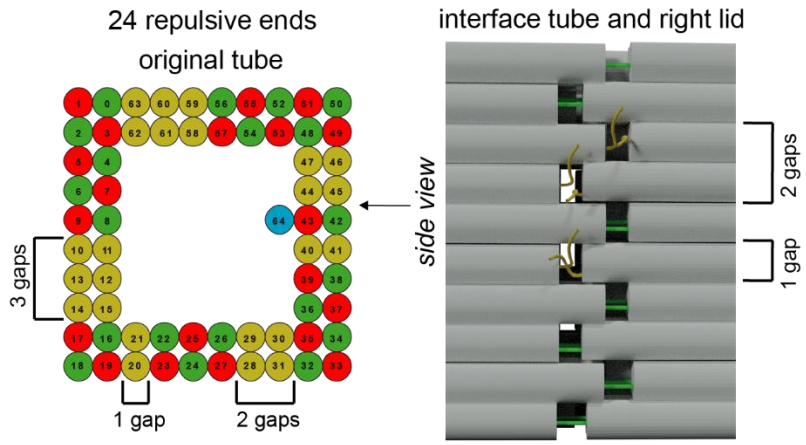

Figure S9 - Gaps at the tube-lid interface from consecutive repulsive DNA ends.

The original tube-lid interface employs 24 repulsive DNA ends. Regions containing multiple consecutive repulsive DNA ends have been identified as preferred sites for the escape of larger cargo molecules (see simulation results in Figure 6). At these positions the DNA ends are rather flexible such that transient gaps for protein escape can be formed. Shown is the distribution of attractive (red and green) and repulsive DNA ends (yellow) of the tube interfaces (left scheme), together with a three-dimensional scheme (right) for the tube-lid docking, viewing the interface sides of the right lid and the right tube side. For the right scheme attractive staple overhangs are shown in green and repulsive overhangs in yellow.

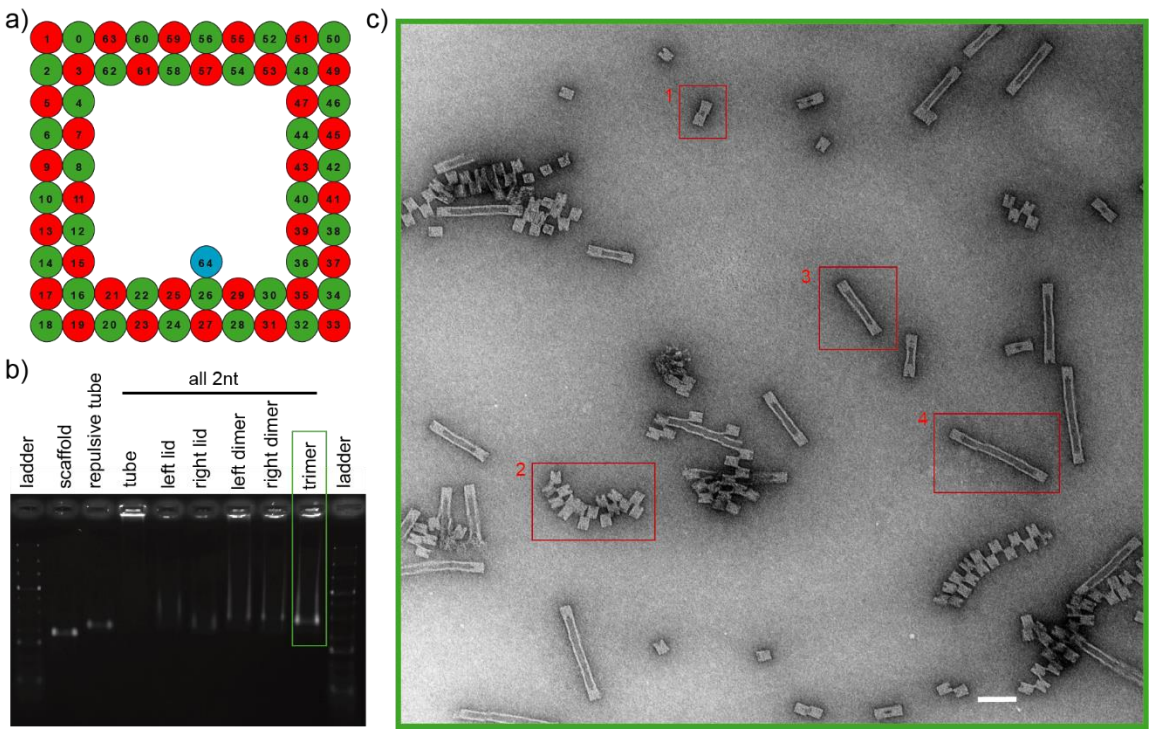

Figure S10 - Cage assembly for interface comprising only attractive DNA ends with 2nt overhangs.

a) Distribution of attractive DNA ends of the tube interfaces with 2 nt recessions (red) and 2nt overhangs (green). **b)** Monitoring the assembly of cages by agarose gel electrophoresis. The DNA is visualized by subsequent ethidium bromide staining. As samples, the scaffold, a repulsive tube with only repulsive DNA ends at the interfaces, as well as the tube and the two lids with the all-attractive interfaces and corresponding dimeric and trimeric mixtures are taken (see legend). Notably for the modified tube version, as well as the dimer and trimer samples large aggregate that became stuck inside the gel wells were formed. **c)** TEM image of the trimer sample revealing significant unspecific interactions between the lids (2) and tubes providing the formation of significantly longer cavities (3, 4). The scale bar corresponds to 100 nm.

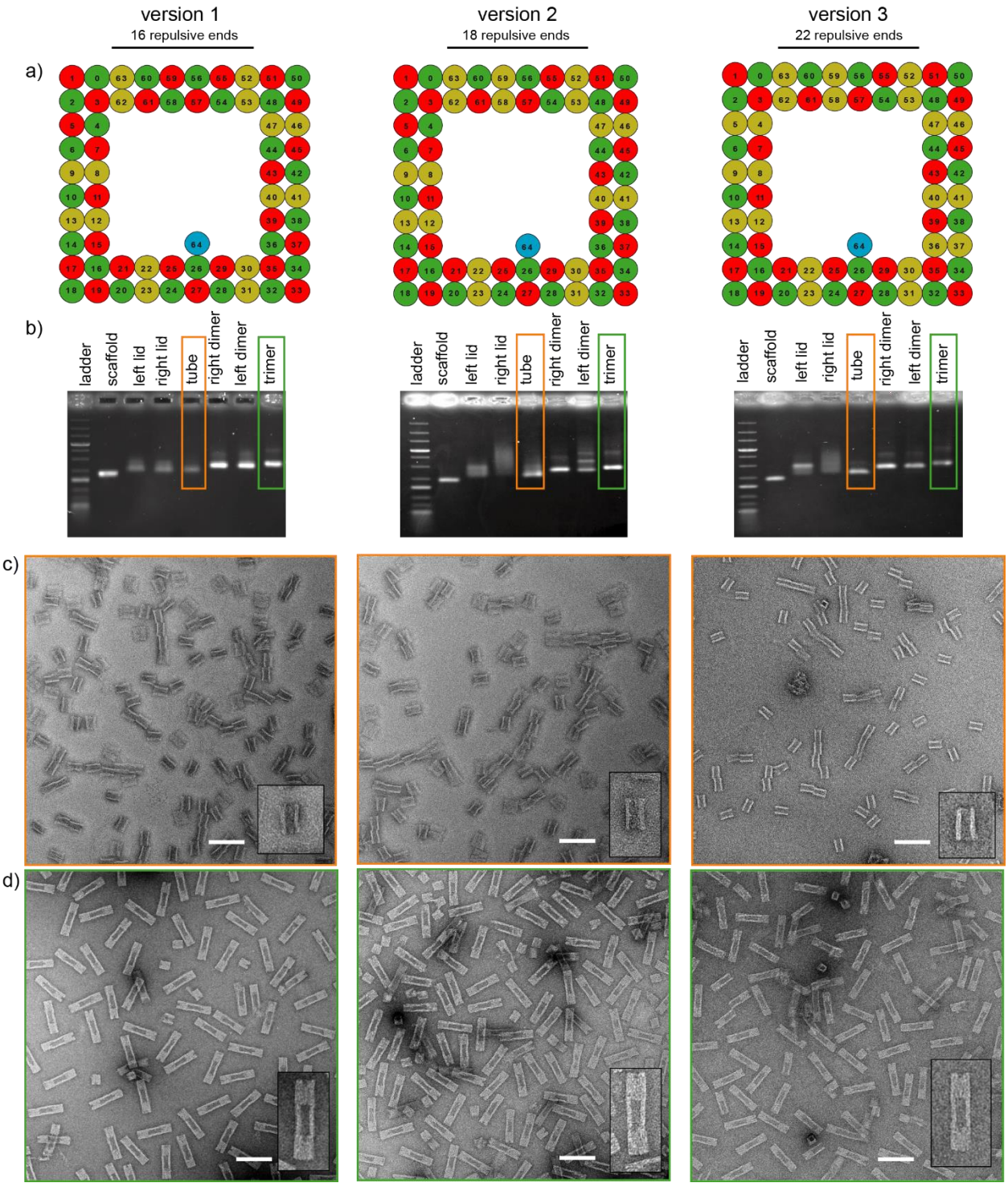

Figure S11 - Assembly of nanocage versions 1, 2 and 3 with tighter tube-lid interfaces.

a) Distribution of attractive (red and green) and repulsive (yellow) DNA ends of the tube interfaces, with 16 repulsive DNA ends for interface of version 1, 18 repulsive ends for interface of version 2 and 22 repulsive ends for interface for version 3. For these interfaces consecutive repulsive DNA ends were

avoided in contrast to the original design. Blue circles inside the tube indicate the target strand. **b)** Analysis of the cage assembly by agarose gel electrophoresis and subsequent ethidium bromide staining. Individual lanes contain (from left to right) a DNA size marker, the scaffold, the individual tube and lid monomers and corresponding dimeric and trimeric mixtures (see legend). For most monomers a single sharp band (particularly for the tubes, see orange box) is observed. Only for some lid monomers of version 2 and version 3 some non-specific multimer formation is observed. For the trimeric mixtures of the tube monomers with the two lids (green box) a single sharp band is obtained for all interface versions indicating a specific and efficient formation of nanocages. **c)** TEM images of the tube monomers with different interface versions revealing only little aggregate formation for version 1 and version 2, when heating the sample to 37 °C (as done during incumbent annealing). **d)** TEM images of the trimeric samples revealing highly efficient cage formation for all interface versions. The scale bars correspond to 100 nm.

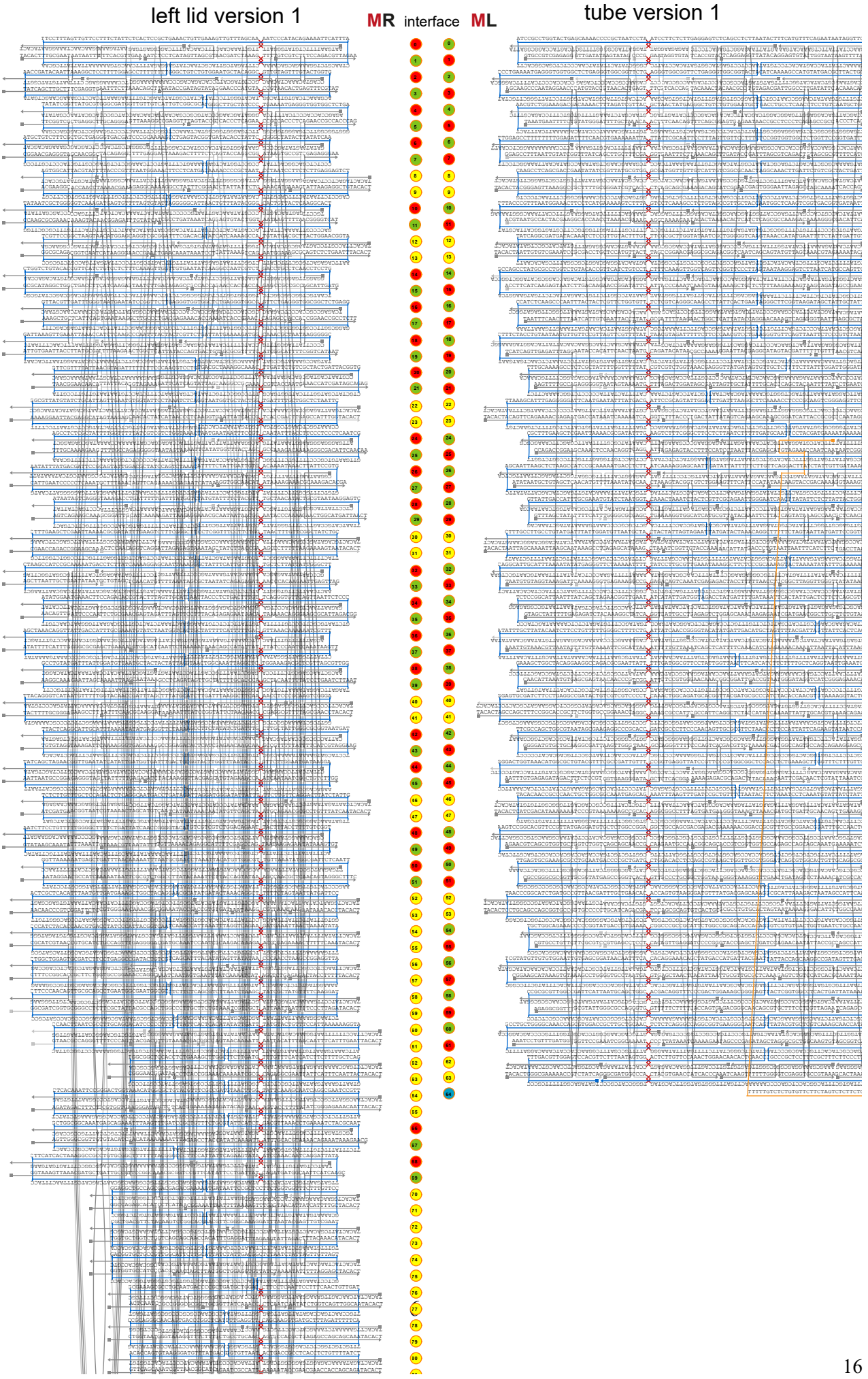
left lid version 1
MR interface ML
tube version 1

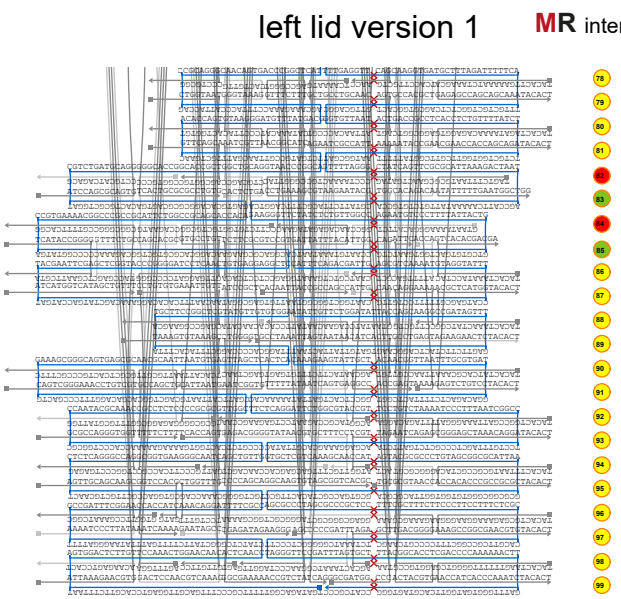

Figure S12 – Design templates of the left side of the origami nanotube and of the left lid in its version 1.

The blue lines show the routing of the scaffolds p8064 with complementary staples in grey. The orange line (starting at helix 24) represents the staple that carries the target strand sequence as a 3'-overhang. Attractive helices ends with 2 nt recessions or extensions are marked with red or green circles, respectively. Yellow circles mark the repulsive helix ends with TACACT overhang. The blue circle in helix 64 marks the 3' overhang of the target strand that protrudes inside the cavitiy of the tube. Red crosses are introduced as imaginary gaps for the graphical illustration. At the left side of the lid only repulive ends are present as shown in the first two lines. The design is based on a square lattice of DNA helices.

tube version 1 **NR** interface **NL** right lid version 1

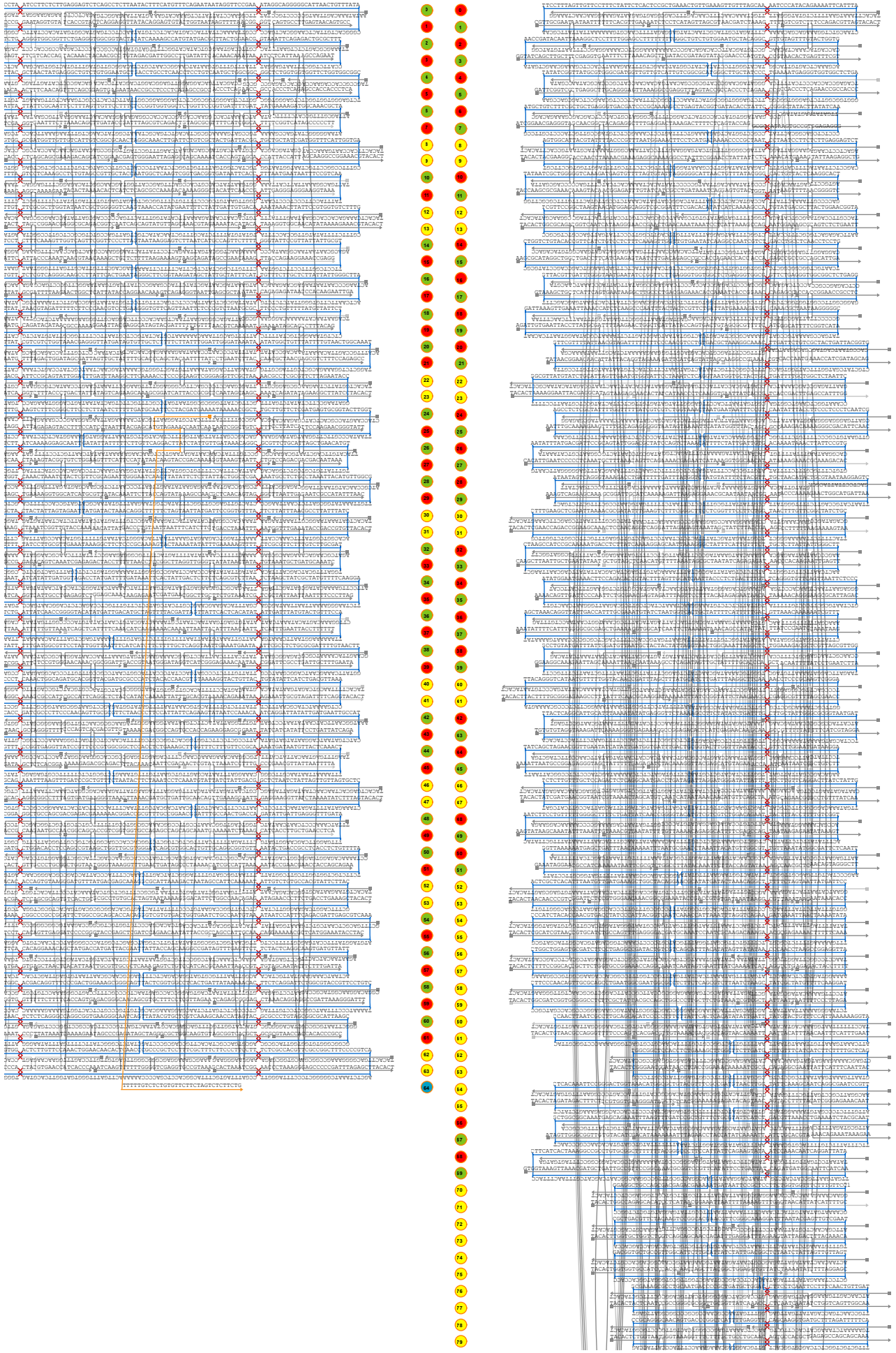

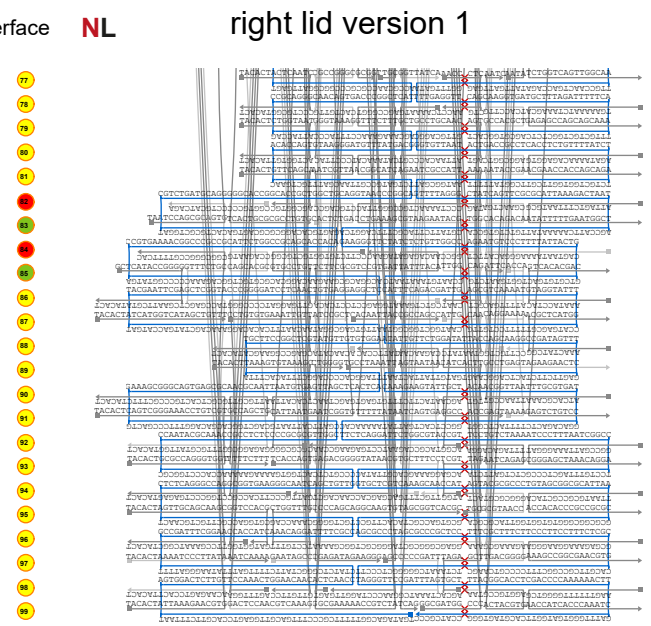

Figure S13 – Design templates of the right side of the origami nanotube and of the right lid in its version 1.

The blue lines show the routing of the scaffolds p8064 with complementary staples in grey. The orange line (starting at helix 24) represents the staple that carries the target strand sequence as a 3'-overhang. Attractive helices ends with 2 nt recessions or extensions are marked with red or green circles, respectively. Yellow circles mark the repulsive helix ends with TACACT overhang. The blue circle in helix 64 marks the 3' overhang of the target strand that protrudes inside the cavitiy of the tube. Red crosses are introduced as imaginary gaps for the graphical illustration. The design is based on a square lattice of DNA helices.

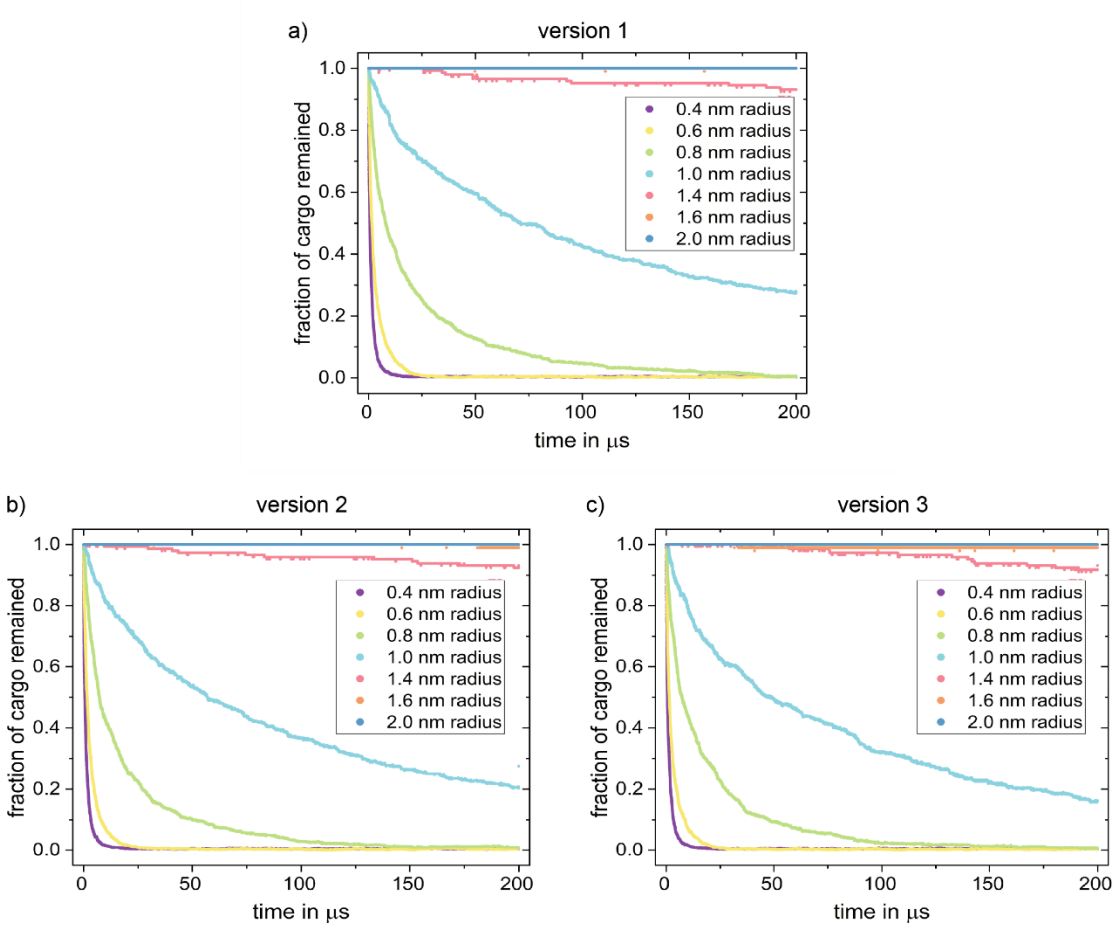

Figure S14 – Simulated release kinetics of differently sized cargo from the nanocage versions 1, 2 and 3.

Shown are the cargo fraction remaining inside the cages as function of time for the different cargo radii simulated for all three new versions (version 1 (a), version 2 (b), version 3 (c). Compared to the original version (Figure 6), the release of streptavidin-incumbent over time is considerably restricted regarding the higher radii.

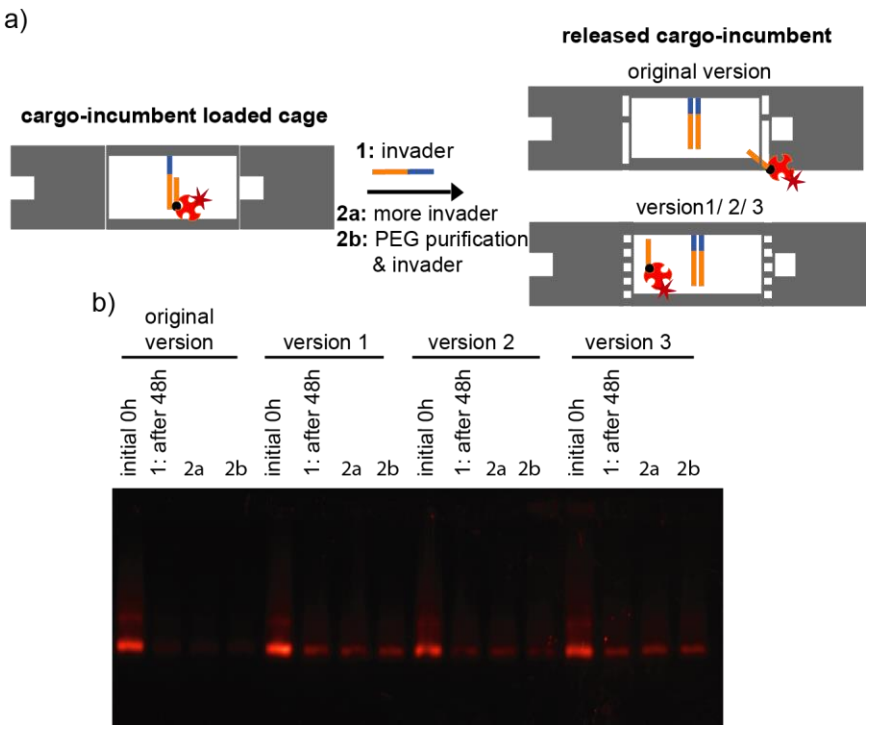

Figure S15 – Control reactions to support the observed retention of unbound streptavidin molecules by the tighter nanocage versions 1 - 3 (see Figure 7).

a) Scheme of the strand displacement reaction using a streptavidin-incumbent and a ssDNA invader. To show that the retention of streptavidin in the original experiment after 48 h (**1**) was not due to insufficient amounts of invader, after 24 h, invader was added to reach a 4:1 excess of invader strands over target strands (**2a**). To exclude that a too high concentration of external free streptavidin-incumbents could influence further escape from the cage, free streptavidin-incumbents were removed 24 h after the initial invader addition by PEG precipitation, followed by an invader addition for another 24 h (**2b**). **b)** Monitoring streptavidin-incumbent release for the original and the improved DNA nanocage versions following the experimental schemes 1, 2a and 2b. The retention of streptavidin-incumbent was measured for all experiments after 48 h. For the altered schemes 2a and 2b the same amount of streptavidin was retained inside the cages indicating that free streptavidin complex could be trapped inside the tight cage versions 1-3.

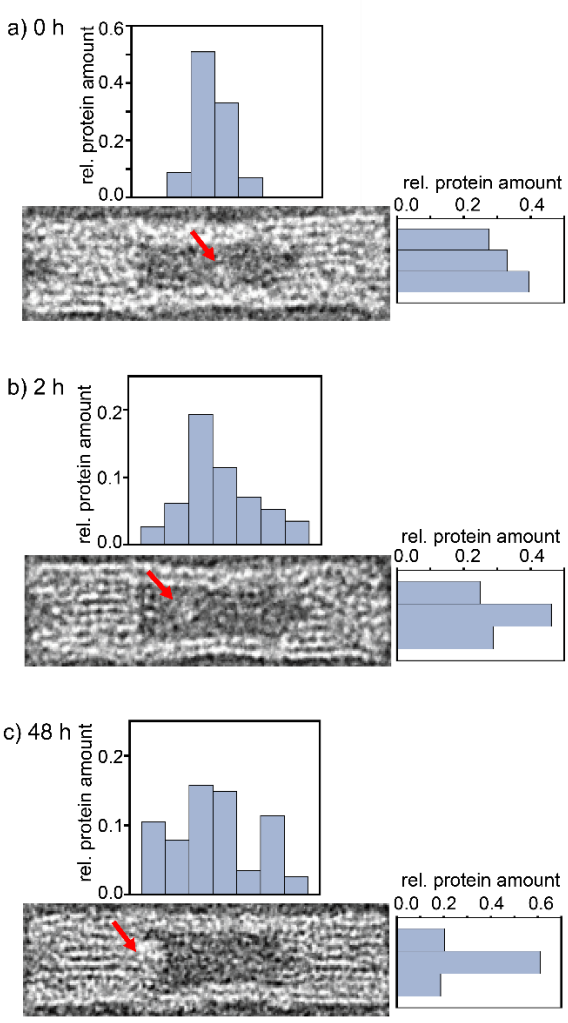

Figure S16 – Localization of streptavidin inside the nanocage cavity of version 1 after streptavidin incumbent loading as well as 2 h and 48 h after DNA invader addition.

Shown are in each subpanel a representative snapshot of a single cage as well as histograms of the position of streptavidin molecules along the long and the short cavity axis of the origami nanocage of version 1. The distribution is obtained from 30-40 origami cages on different TEM images after streptavidin-incumbent loading (a) as well as 2 h (b) and 48 h (c) after invader addition (see Figure 7). The cage cavity is divided into seven bins along the long and three bins along the short axis and the protein position was attributed to particular bins by visual inspection of the individual nanocages images.